Seismic response of offshore wind turbine supported by monopile and caisson foundations in undrained clay

Maosong Huang[1,2]✉, He Cui[1,2], Zhenhao Shi[1,2], and Lei Liu[1,2]

[1] Key Laboratory of Geotechnical and Underground Engineering of Ministry of Education, Tongji University, China
[2] Department of Geotechnical Engineering, Tongji University, China
mshuang@tongji.edu.cn

Abstract. The seismic performance of offshore wind turbine (OWT) becomes increasingly critical as more wind farms are built/planned in sites subjected to active seismic events. Time-domain, continuum-based methods can provide comprehensive analyses of OWT during seismic shaking yet its application in engineering practice can be restricted by the complexity of soil constitutive models. This work presents a constitutive model for undrained clay that is simple yet replicates the essential soil behavior, including mechanical anisotropy, cyclic degradation of stiffness and strength, and path-dependent stiffness nonlinearity at small strains. The capacity of the soil model is assessed at various levels, by simulating soil element tests, the response of cyclically-loaded pile in centrifuge test, and the response of caisson-supported OWT in seismic centrifuge test. These assessments show that the seismic response of OWT can be reasonably represented by the proposed method. Based on the soil model, dynamic finite element analyses are performed to explore the seismic response of OWT supported by different foundation types: monopile and caisson. This investigation highlights: (1) the dynamic response of OWT foundation is governed by the kinematic-inertia interactions between soil, foundation, and superstructures; (2) the resonance of OWT structure system (including higher modes) can be a critical mechanism behind the developments of excessive foundation movements.

Keywords: Offshore wind turbine foundations, Monopile, Caisson, Seismic response, Constitutive relations

1 Introduction

The offshore wind sector represents an essential component for delivering large-scale, affordable, and clean energy [1]. Due to their harsh working environments, the foundation of offshore wind turbine (OWT) is required to sustain substantial cyclic lateral loading, e.g., wind and wave actions. Accordingly, the above aspect has been subjected to substantial investigations (e.g., see [2-4]). In the contrast, the seismic response of OWT foundations was traditionally considered secondary, largely due to the intrinsic flexibility of OWT structures and the typical frequency contents of earthquakes

[5]. This aspect, nevertheless, has begun to gain increasing attention from both academics and practitioners [6-12], due to the exponential expansion of offshore wind farms worldwide and, consequently, more frequent overlap between the active seismic regions and wind farms sites [6]. This paper has been focused on the seismic response of OWT supported by monopile and suction caisson, i.e., predominant OWT foundation types [3, 13-18].

Literature on the seismic response of OWT is not as extensive as that for the case of cyclic lateral response. Nevertheless, several trends have been gradually recognized. The OWT structures display inherent flexibility and their fundamental natural frequency typically is around 0.25 to 0.75 Hz [3, 6]. This range circumvents the frequency content of typical earthquakes that corresponds to the strongest excitation and makes the risk of earthquake-induced catastrophic collapse relatively low. Among 180 real earthquake records, De Risi et al. [6] show that only two lead to structural failure of OWT. Similar behavior is reported by other seismic fragility analyses [19, 20]. On the other hand, it should be emphasized that higher vibration modes can play important roles in affecting the seismic response of OWT [6, 10, 21, 22], because the corresponding resonance frequencies can coincide with those characterized by strong ground motions. The involvement of higher vibration modes can potentially shift the distributions and patterns of internal force demands [21, 22] and require special care in OWT structure design.

While the chance of the collapse of OWT during earthquake might be low, excessive deformation of OWT and exceeding the serviceability limit state (SLS) can be an important issue [6, 7, 10, 23]. For instance, Gao et al. [23] show that, in the liquefiable ground, OWT caisson foundation can develop considerable residual rotation (i.e., up to 40% of SLS) solely due to earthquakes. Kourkoulis et al. [7] and Anastasopoulos and Theofilou [10] show that, in undrained clay, OWT caisson and monopile foundation can rotate significantly during seismic shaking, however, it is transient and largely recoverable by the end of earthquake. An important factor that affects the deformation of OWT during earthquake is the coupling between seismic excitation and environmental actions. Kourkoulis et al. [7] and Anastasopoulos and Theofilou [10] show that the presence of wind and wave loads can significantly enlarge the accumulation of OWT foundation rotations during earthquake. Zheng et al. [24] and Yang et al. [25] show that the inclusion of wave actions can increase the seismic response of OWT structures. Another factor that can influence the OWT deformation is the frequency contents of seismic excitations. The foundation deformation and structure response can both be amplified when earthquake displays more intense motion at the natural frequency of OWT structure system [6, 26].

The seismic behavior of OWT is complex and governed by many factors. Among them, accurate modeling of soil-structure interaction (SSI) has been shown essential for predicting the performance of OWT during earthquake. The latter aspect has been considered by two main approaches: Winkler spring-based models [6, 25, 27] and continuum-based models [7, 10, 26]. The former method is attractive from the per-

spective of simplicity. Nevertheless, its reliability highly depends on the employed soil reaction curves, which can be empirical and limited to certain applications. Moreover, Winkler spring-based models often cannot accurately consider the near-field ground shaking that is affected by the presence of foundation.

Time-domain, continuum-based approaches (e.g., finite element analysis (FEA)) can naturally account for the seismic wave propagations in the ground and the kinematic-inertia interactions between soil, foundation, and superstructures. Despite these advantages, the investigations using continuum analysis are limited, compared to the counterparts of Winker spring-based methods. This at least partially results from the complexity of the method, which might be to a large extent attributed to the complexity of the constitutive models for soils. The goal of this paper is to show the possibility of delivering realistic and efficient FEA of the seismic response of OWT based on the constitutive models that are simple yet captures essential features of soil behavior. In the following, one of such models for undrained clay will be described, followed by the assessment of its capacity to represent cyclic soil-structure interactions against cyclic lateral loading and seismic shaking centrifuge tests. Lastly, dynamic FEA based on the soil model is performed to explore the seismic response of OWT supported by different foundation types: monopile and caisson.

2 Total stress-based constitutive model for undrained clay

In many built and planned OWT farms, fine-grained soils constitute the primary seabed [13, 17, 28]. Given the low permeability of the clayey soils, undrained conditions are often prevailing during earthquake. This study idealizes undrained clay as a single-phase material governed by total stresses. The formulation of the total stress model will be briefly described in this section, followed by examples illustrating its capacity to represent the behavior of cyclically-loaded undrained clay.

2.1 Model formulation

The employed total stress soil model (hereafter referred to as AUC-Clay-Small) can capture the salient features of undrained clay, including mechanical anisotropy, cyclic degradation of stiffness and strength, and path-dependent nonlinear variation of stiffness at small strains. More detailed description of the constitutive model can be found from the authors' previous publications [29-31].

The AUC-Clay-Small model employs a Mises type yield surface (see $f = 0$ in Fig. 1):

$$f = \sqrt{\frac{3}{2}} \| S_{ij} - \alpha_{ij} \| - A = 0 \tag{1}$$

where S_{ij} indicates the deviatoric stress, α_{ij} denotes the backstress controlling the translation of the yield surface, while the constant A indicates the size of the yield surface.

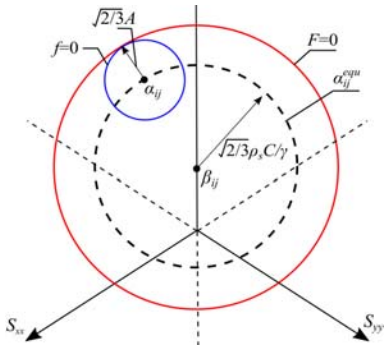

Fig. 1. Schematics illustrating yield surface $f = 0$ and anisotropic strength surface $F = 0$.

The evolution of the backstress is controlled by a nonlinear kinematic hardening law proposed by Huang et al. [29] that accounts for the anisotropy of undrained clay and its cyclic softening:

$$\dot{\alpha}_{ij} = \langle \lambda \rangle \left[\frac{2}{3} \rho_e \rho_s C \frac{\partial f}{\partial \sigma_{ij}} - \rho_e \gamma (\alpha_{ij} - \beta_{ij}) \right] \tag{2}$$

In Eq. (2), λ indicates the plastic multiplier, while C and γ are material constants. The tensor β_{ij} in Eq. (2) accounts for the anisotropic shear strength in that it implies a strength surface that is centered around β_{ij} (see $F = 0$ in Fig. 1). The variables ρ_e and ρ_s are included to consider the cyclic degradation of soil stiffness and strength (see Huang et al. [29] for detailed discussion).

The elastic response of undrained clay is described by an intergranular strain elastic model [30]:

$$G = \rho^{\chi} G_0 + (1 - \rho^{\chi}) G_0 + \begin{cases} \rho^{\chi} |l|^n (G_e - G_0) & \text{if} \quad l > 0 \\ 0 & \text{if} \quad l \le 0 \end{cases} \tag{3}$$

where G indicates the elastic shear modulus, while G_0 and G_e indicate the value of G at very small strains (e.g., less than 1×10^{-5}) and relatively large strains (e.g., greater than 1×10^{-2}), respectively. The transition from G_0 to G_e depends on both the magnitude of shear strains and the rotation of current loading path from the previous history, as observed from experiments [32, 33]. This objective is realized by employing the intergranular strain ζ_{ij} as a state variable for memorizing deformation history.

In general, the modulus G computed by Eq. (3) will decrease from G_0 to G_e during monotonic loading, attain enhanced stiffness upon strain path rotation, and regain the highest stiffness, i.e., G_0, upon full stress reversal. More detailed discussion of the intergranular strain elastic model can be found from [30, 31].

2.2 Simulation of soil element tests

Figure 2 compares the measured and simulated response of Cloverdale clays from undrained triaxial cyclic shear tests [31, 34, 35]. It is seen that the soil model can well represent the cyclic softening observed in the tests (i.e., enlarged and rotated stress-strain hysteresis loops). Moreover, the model can reasonably capture the soil response under cyclic loading with different amplitudes. This feature is further illustrated in Fig. 3, which depicts the observed and computed residual strains (i.e., those attained at the end of each cycle) versus the number of cycles.

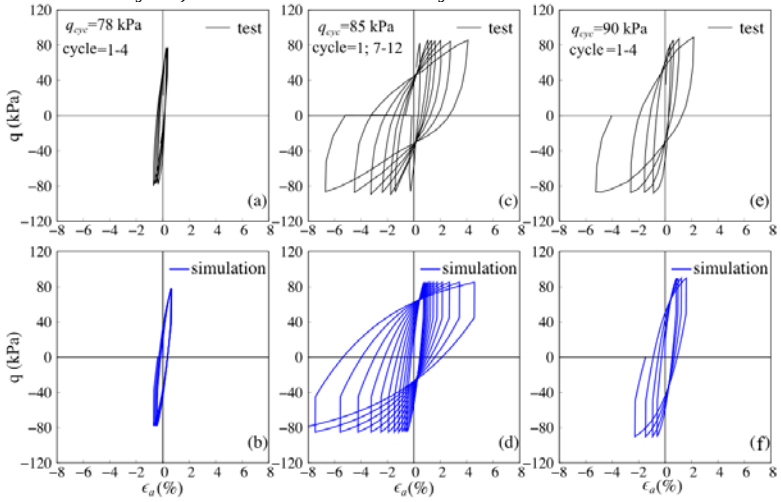

Fig. 2. Measured and simulated response of Cloverdale clay from undrained cyclic triaxial tests: (a)-(b) cyclic shear stress q_{cyc} = 78 kPa; (c)-(d) q_{cyc} = 85 kPa; (e)-(f) q_{cyc} = 90 kPa.

3 Analyses of cyclically-loaded pile in centrifuge test

The application of the total stress model in cyclic soil-structure interaction is demonstrated by simulating a series of centrifuge tests where pile foundations are subjected to cyclic lateral loading [36, 37]. The soils used in the tests are Malaysia kaolin clays. The variation of shear modulus and damping ratio of the soils at small strains, measured by using resonant column tests, are given in Fig. 4. This figure also includes the corresponding model simulations [31].

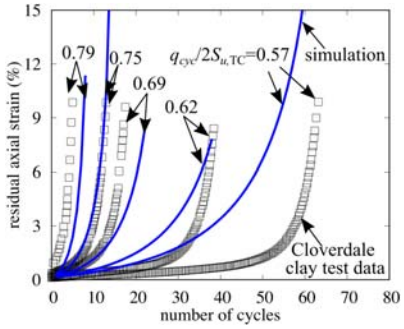

Fig. 3. Measured and computed residual strain versus number of cycles.

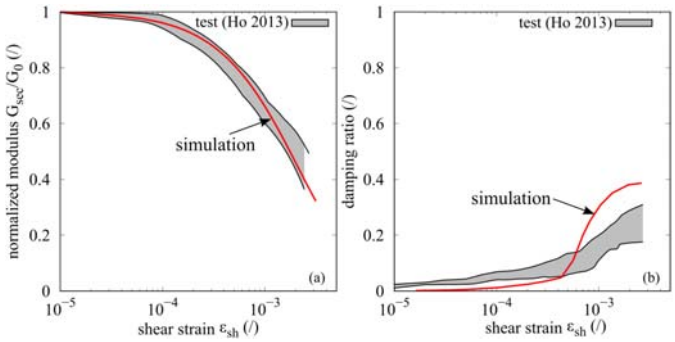

Fig. 4. Small-strain characteristics of Malaysia kaolin clay: (a) shear modulus; (b) damping.

Figure 5 presents the load-displacement relationships at pile head measured from centrifuge tests and computed by FEA based on the AUC-Clay-Small model (detailed discussion on the FEA mesh and boundary conditions can be found from [29]). The graphs (a) and (b) show the response of the semi-rigid pile with a free head subjected to small and large magnitudes of cyclic pile head displacements, respectively, while the graphs (c) and (d) show the counterpart for the rigid pile with a fixed head. It is seen that the measured hysteresis can be reasonably represented by the FEM simulations, as well as the gradual drop of pile head reactions at peak displacement during cyclic loading (i.e., the softening of pile foundation stiffness).

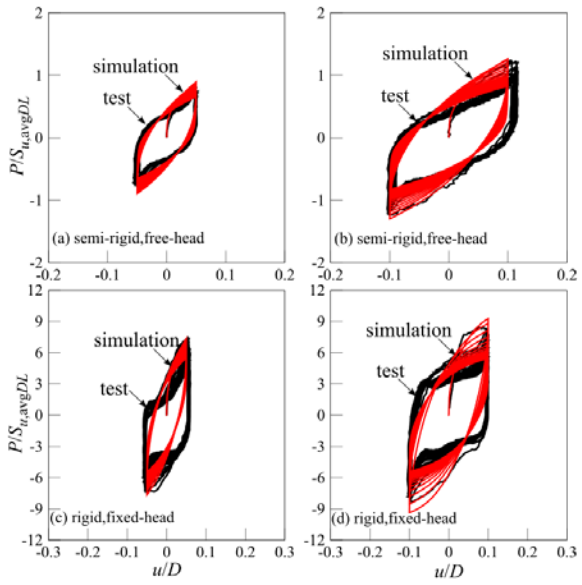

Fig. 5. Measured and computed load-displacements at pile head from centrifuge test.

4 Analyses of caisson supported OWT in seismic centrifuge test

The total stress soil model described in Section 2 is incorporated into time-domain, dynamic finite element analysis (FEA) and is applied to simulate a seismic centrifuge test of OWT. The test is conducted at TJL-150 centrifuge facility at Tongji University. A laminar box (550 mm in height, 500 mm in both length and width) is used to contain the soils (see Fig. 6(a)). The earthquake loading is applied under a centrifuge acceleration of 50 g. The model OWT is simplified as a one-degree-of-freedom system, where an aluminum tube (inner and outer diameters are 0.9 m and 1.0 m, respectively, in prototype size) and a concentrated mass (5.47×10^3 kg, in prototype size) are used to represent the turbine tower and the rotor-nacelle head, respectively. The OWT foundation is a caisson with a diameter of 4.2 m and an embedment depth of 4.2 m (prototype size). The test is instrumented by accelerometers (A1 to A4 in Fig. 6(a)) and LVDTs (L1 and L2 Fig. 6(a)). The soils used in the centrifuge test are the normally consolidated Malaysia kaolin clays discussed in the previous section.

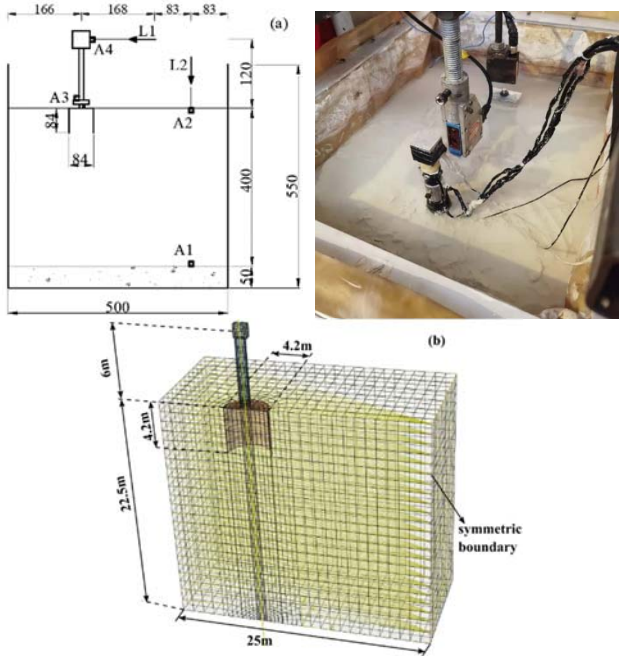

Fig. 6. Layout of (a) seismic centrifuge test and (b) dynamic FEA.

Figure 6(c) shows the mesh used in the FEA. To simulate the laminar box, the degrees of freedom at the same elevations along the opposite sides of the model perpendicular to the excitation direction are tied together (i.e., symmetric boundary). The degrees of freedom at the nodes along the other two sides are fixed along the normal direction. At the base of the FEA model, all degrees of freedom are fixed except the one along the direction of earthquake excitation, for which the acceleration input in the centrifuge test (see Fig. 7) is prescribed.

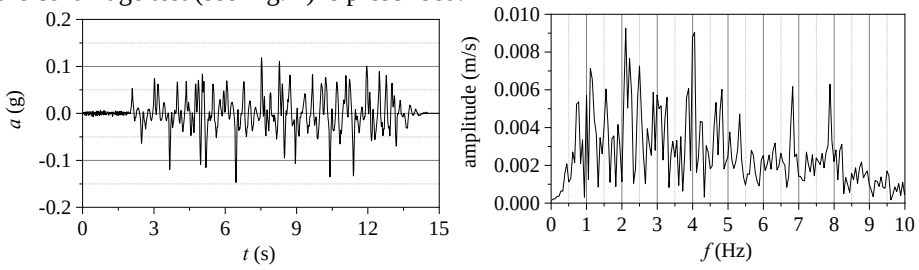

Fig. 7. Input acceleration in centrifuge test: (a) time history; (b) spectrum.

Figures 8 to 10 show the measured acceleration at the ground surface (A2 in Fig. 6(a)), caisson foundation near mudline (A3 in Fig. 6(a)), and the OWT tower header (A4 in Fig. 6(a)), respectively. The comparison between Fig. 8(a) and 9(a) shows that the ground motion is attenuated during upward propagation, in particular, high frequency contents. This might be attributed to the low shear strength of normally con-

solidated clays near ground surface. Fig. 9 shows that the acceleration of the caisson foundation is de-amplified relative to ground motion. In contrast to the foundation response, Fig. 10 shows that the OWT tower head exhibits considerable amplification in relative to that of the ground surface. The FEA computations are also included in Figs. 7 to 9, which can reasonably represent the above general trends observed from the experiments. It is noted that the FEA can reasonably capture the frequencies of local peak response of the OWT header (see Fig. 10(c) and (d)), but tends to over-estimate the overall amplitudes. This discrepancy might suggest that the adopted soil parameters (i.e., determined solely based on the cyclic loading centrifuge test discussed in Section 3) can over-estimate the stiffness and strength of the soils used in the seismic centrifuge test.

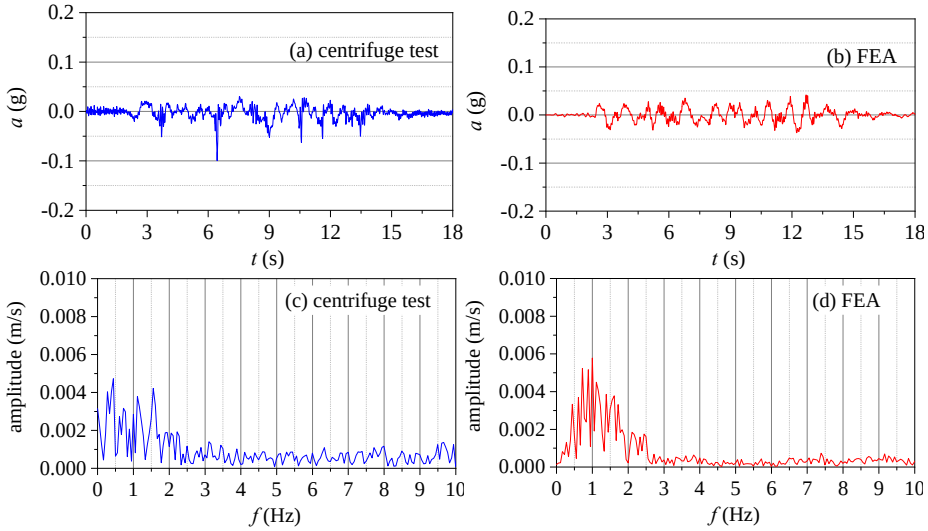

Fig. 8. Measured and computed acceleration response at ground surface: (a)-(b) time history; (c)-(d) spectrum.

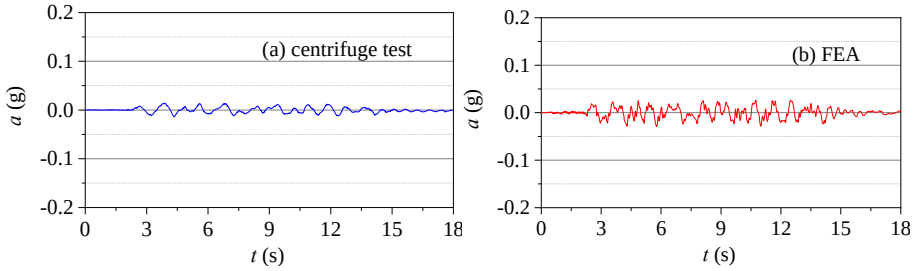

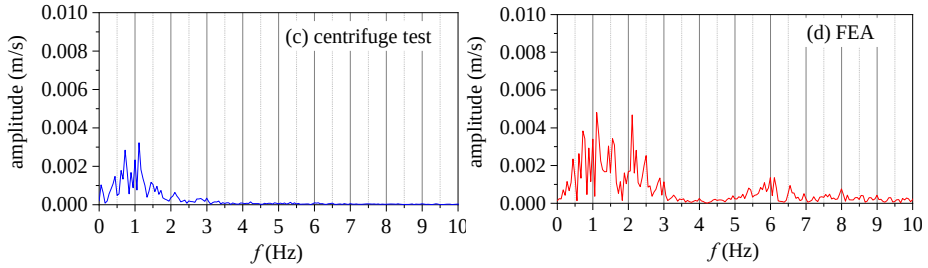

Fig. 9. Measured and computed acceleration response of caisson near mudline: (a)-(b) time history; (c)-(d) spectrum.

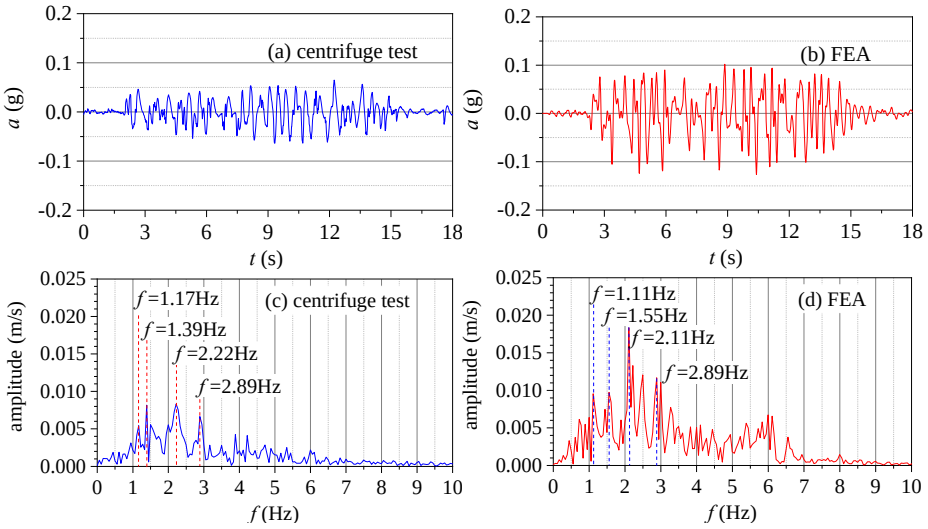

Fig. 10. Measured and computed acceleration response of OWT tower header: (a)-(b) time history; (c)-(d) spectrum.

Figure 11 presents the measured and computed ground settlement and lateral movement of OWT header during seismic shaking. The FEA can reflect the gradual development of surface settlement and OWT displacement observed from the centrifuge test, but under-estimate the overall magnitude. This mismatch is consistent with those regarding the acceleration response (e.g., Fig. 10) and, as discussed above, might be explained by that the actual soil properties in the centrifuge test are weaker than those implied by the soil parameters adopted in the FEA.

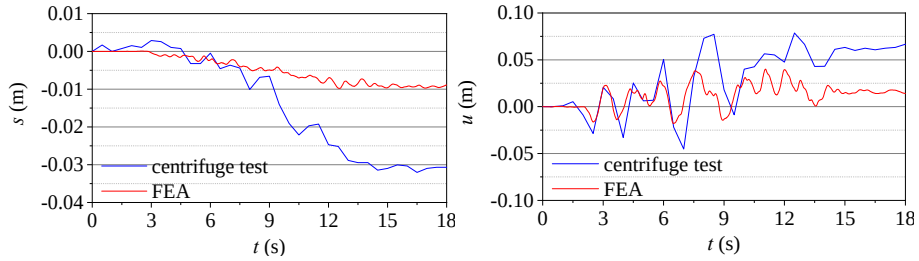

Fig. 11. Measured and computed time history of (a) ground surface settlement and (b) OWT header lateral movement (prototype scale).

5 Seismic response of OWT supported by different foundation types

Previous sections show the capacity of FEA based on the simple soil model to represent the performance of OWT during earthquake loading. In this section, this numerical tool is used to explore the influences of foundation types on the seismic response of OWT. For this purpose, monopile and caisson foundation are considered (see Fig. 12). The superstructure is a simplified representation of typical 5 MW OWT installed in China. The tower is modeled as a steel hollow cylinder (outer and inner diameters are 6 m and 5.84 m, respectively; the density is 7.8×10^3 kg/m^3), while the rotor-nacelle head is simplified as a concentrated mass (267.8 Tons). The sizes of the caisson foundation are chosen in accordance with those adopted in an OWT farm in China. The sizes of the monopile are adjusted to match the lateral stiffness of the caisson foundation near the mudline in preliminary static elastic analysis. Infinite elements are prescribed along the lateral sides of the FEA mesh to minimize wave reflections. The acceleration time history prescribed at the bottom of the model is given in Fig. 13. The soils adopt the parameters used in the above centrifuge test but follow a different profile of shear modulus $G_0 = 7 + 4.35z$ MPa/m and undrained shear strength $S_u = 20 + 2z$ kPa/m, respectively. The gradient of these profiles is close to in situ measurements in Shanghai area. To reduce the computational cost, the proposed total stress model is approximated by a built-in kinematic hardening model in Abaqus, in conjunction with a user-defined field for cyclic softening of stiffness and strength. By doing so, the mechanical anisotropy of undrained clay and the path-dependent non-linearity at small strains is neglected. Figs. 14 and 15 suggest that such a simplification (denoted by AUC-Clay) does not lead to significant alteration of the general patterns of computed response.

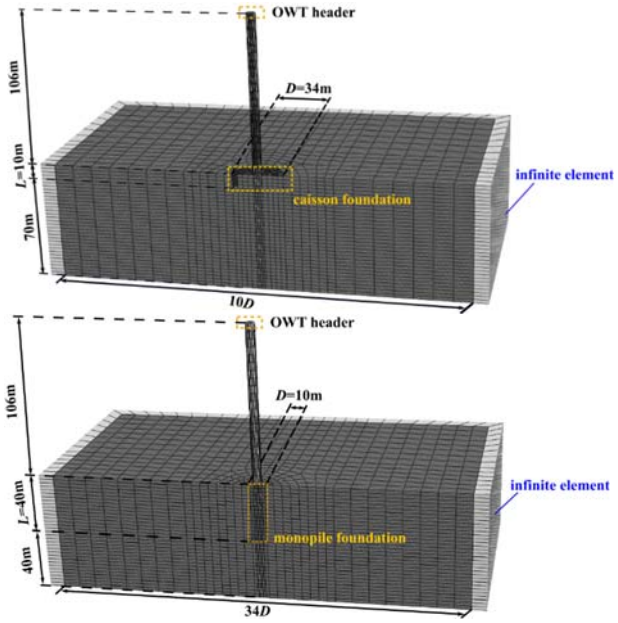

Fig. 12. FEA model of OWT supported by: (a) caisson; (b) monopile. Note that only half of the model is depicted to show the location of the foundations.

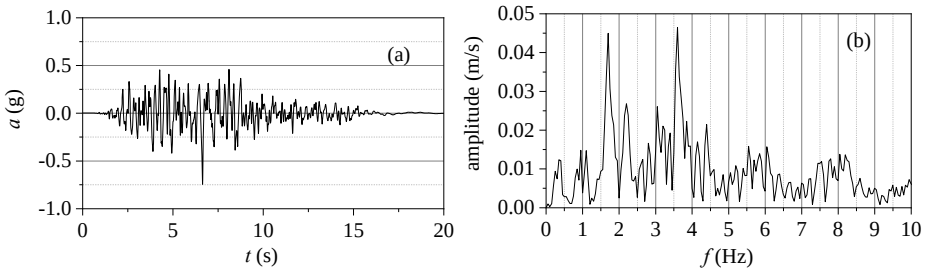

Fig. 13. Input acceleration at the base of FEA model: (a) time history; (b) spectrum.

Fig. 14. Acceleration response of monopile at mudline computed by two soil models: (a) AUC-Clay; (b) AUC-Clay-Small.

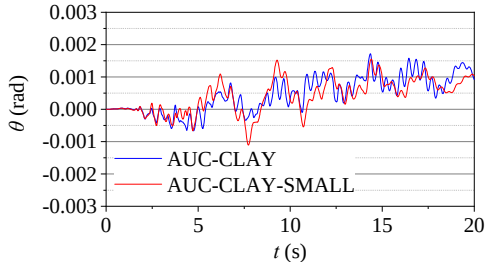

Fig. 15. Rotation of monopile at mudline computed by using AUC-Clay and AUC-Clay-Small model.

Figures 16 and 17 show the acceleration response of the ground surface (at locations relatively far from the foundation) and the two types of foundation at the mudline, respectively. In general, the presence of foundation de-amplifies the ground motion, similar to that observed from the centrifuge test. The comparison between Fig. 16(b), 17(d) and 17(d) shows that the above filtering is more significant for high-frequency contents, indicating that it is caused by the kinematic interaction between foundation and ground, i.e., the high stiffness of the foundation in relative to the ground makes it cannot follow the high-frequency vibration of the ground [38]. Moreover, the monopile has stronger filtering effects than the caisson foundation (see Fig. 17(b) and (d)), suggesting that the former foundation is stiffer. Fig. 18 shows the ratio between the displacement amplitude of foundation and ground surface under different excitation frequencies. It is seen that, despite the above filtering effects, the response of foundation is amplified under certain frequencies.

Fig. 19 shows the acceleration response of the OWT header. For the caisson-supported OWT, local peak amplifications are seen at 0.2 Hz and 2.05 Hz, close to the range of the first and second natural frequency of typical OWT structure system [6], indicating these local peaks are caused by the resonance. Moreover, Fig. 19(b) shows that the resonance at the second mode leads to a greater OWT response than that of the first mode, thus suggesting that sufficient attention should be paid to higher modes of OWT structure during seismic analysis. Similar trends are also observed for the monopile-supported OWT (i.e., Fig. 19(c) and (d)), except that the natural frequencies tend to be greater. This is consistent with the above-mentioned fact that the monopile is stiffer than the caisson. Comparing Figs. 18 and 19 shows that, under excitation frequencies close to the second natural frequency of OWT structure, the foundation response is amplified relative to the reference free-field conditions, i.e., the inertial interaction between foundation and superstructures [38].

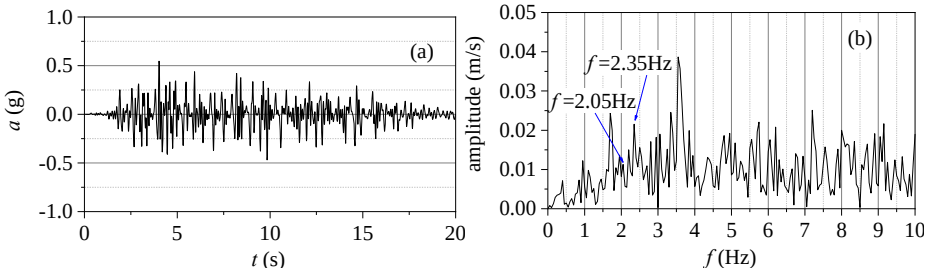

Fig. 16. Free-field ground surface acceleration: (a) time history; (b) spectrum.

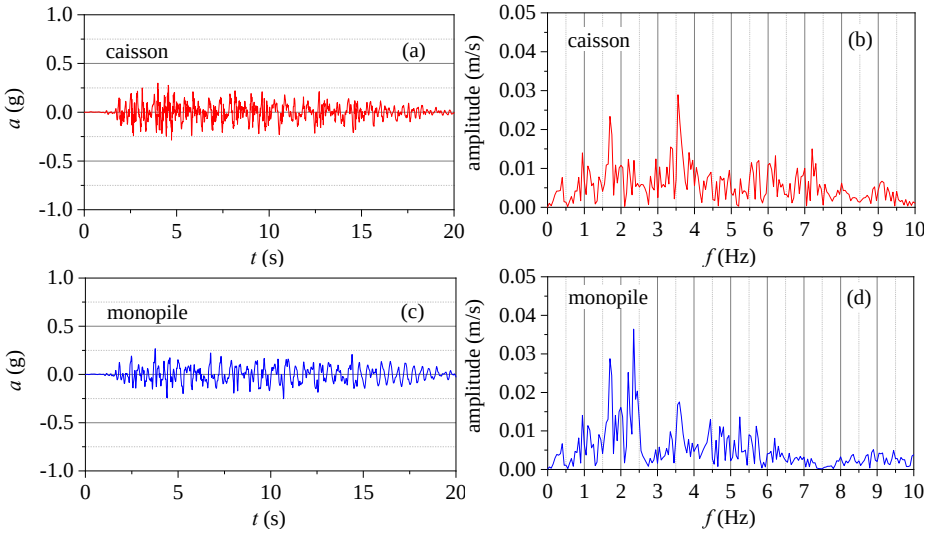

Fig. 17. Acceleration response of foundation at mudline.

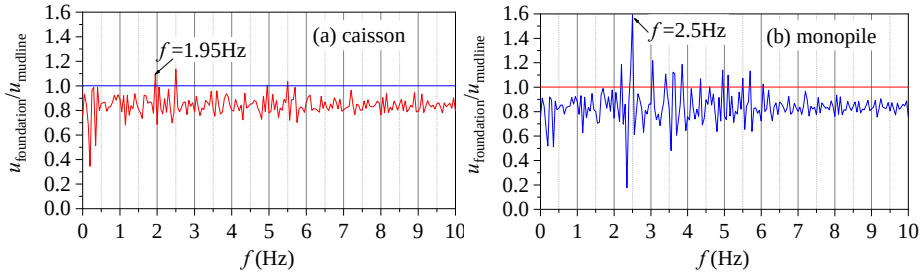

Fig. 18. Ratio between displacement amplitude of foundation and ground surface.

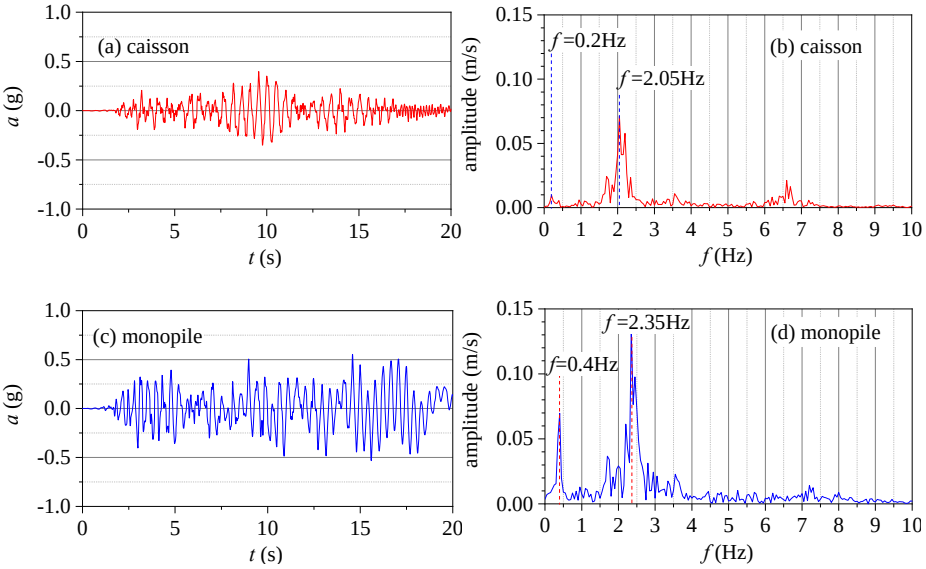

Fig. 19. Acceleration response of OWT header.

Figure 20(a) shows the time history of the ground settlement and foundation settlement during seismic shaking. The caisson foundation settles following that of its surrounding soils. In contrast, the monopile settles less than the ground. Fig. 20(b) shows the time history of foundation rotation. It should be emphasized that, despite that the monopile displays greater stiffness than the caisson (i.e., larger natural frequency in Fig. 19), it develops considerably greater residual rotation than the caisson. This response can be attributed to the relationships between the frequency contents of the ground motions and the natural frequency of the OWT system. The comparison between Fig. 16 and 19 shows that the ground shaking at the second natural frequency of the monopile-supported OWT (f=2.35 Hz) is larger than that of the caisson-supported OWT (f=2.05 Hz). Therefore, avoiding resonance of OWT system including higher modes can be important for preventing excessive deformation of OWT foundations.

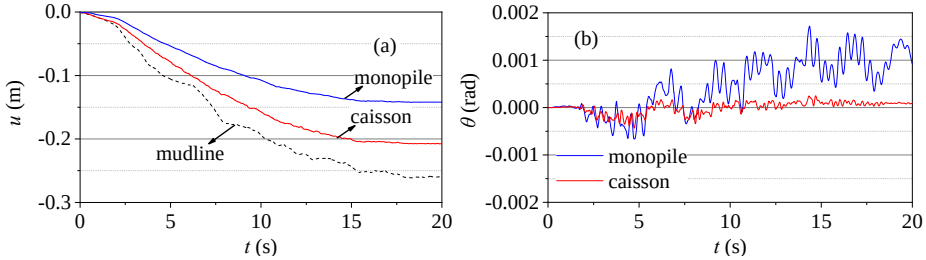

Fig. 20. Time history of (a) foundation and ground settlements and (b) foundation rotation.

6 Conclusions

The seismic performance of offshore wind turbine (OWT) becomes increasingly critical as wind farms expand to seismically active areas. Time-domain, continuum-based methods (e.g., finite element analyses, FEA) can provide comprehensive analyses of the performance of OWT subjected to earthquake loading, yet their practical applicability can be restricted by the complexity of the soil constitutive models. This work illustrates the possibility of delivering realistic and efficient continuum analysis based on constitutive models that are simple but capture the essential features of soil behavior. For this purpose, undrained clay is idealized as single-phase material governed by total stresses. Non-linear kinematic hardening is used to reflect mechanical anisotropy and the cyclic degradation of soil stiffness and strength, while intergranular-strain based elastic model is employed to reflect path-dependent stiffness non-linearity at small strains. The soil model is verified at different levels, by simulating soil element tests, the response of cyclically-loaded pile foundation in centrifuge test, and the response of caisson-supported OWT in seismic centrifuge test. Lastly, the soil model is applied to analyze the influences of foundation types, i.e., monopile and caisson, on the seismic performance of OWT. The main conclusions that can be drawn from this study include:

- The proposed continuum method can reasonably represent foundation load-displacement hysteresis and stiffness degradation during cyclic loading, as well as the response of OWT during seismic loading.
- The kinematic-inertial interactions between soils, foundations, and superstructures can govern the response of OWT foundation during seismic loading.
- Higher vibration modes can be important for the dynamic response of OWT and the accumulation of foundation deformation.
- Foundations displaying high stiffness during static loading might, otherwise, lead to a more intense dynamic response of OWT and larger foundation deformation, depending on the frequency contents of seismic shaking.
- Avoiding resonance of OWT structure system (including higher modes) can be important for preventing excessive foundation deformation.

References

1. GWEC, Global Wind Energy Council. Global wind report, 2021 annual market update. Brussels, Belgium (2021).
2. Byrne, B.W., McAdam, R.A., Beuckelaers, W.J., Burd, H.J., Gavin, K., Houlsby, G.T., et al.: Cyclic laterally loaded medium scale field pile testing for the PISA project. In: 4th International Symposium on Frontiers in Offshore Geotechnics, pp. 1323-1332 (2020).
3. Lombardi, D., Bhattacharya, S., Wood, D.M.: Dynamic soil–structure interaction of monopile supported wind turbines in cohesive soil. Soil Dynamics and Earthquake Engineering 49, 165-180 (2013).

4. Achmus, M., Kuo, Y-S., Abdel-Rahman, K.: Behavior of monopile foundations under cyclic lateral load. Computers and Geotechnics 36(5), 725-735 (2009).
5. Bhattacharya, S., Goda, K.: Use of offshore wind farms to increase seismic resilience of nuclear power plants. Soil Dynamics and Earthquake Engineering 80, 65-68 (2016).
6. De Risi R., Bhattacharya, S., Goda, K.: Seismic performance assessment of monopile-supported offshore wind turbines using unscaled natural earthquake records. Soil Dynamics and Earthquake Engineering 109, 154-172 (2018).
7. Kourkoulis, R., Lekkakis, P., Gelagoti, F., Kaynia, A.: Suction caisson foundations for offshore wind turbines subjected to wave and earthquake loading: effect of soil–foundation interface. Géotechnique 64(3), 171-185 (2014).
8. DNV, Det Norske Veritas. Design of offshore wind turbine structure. Offshore Standard DNV-OS-J101 (2004).
9. IEC, International Electrotechnical Commission. IEC 61400-3 wind turbines Part 3: design requirements for offshore wind turbines. International Electrotechnical Commission, Geneva, Switzerland (2009).
10. Anastasopoulos, I., Theofilou, M.: Hybrid foundation for offshore wind turbines: Environmental and seismic loading. Soil Dynamics and Earthquake Engineering 80, 192-209 (2016).
11. Herrera, J., Aznárez, J.J., Padrón, L.A., Maeso, O.: Observations on the influence of soil profile on the seismic kinematic bending moments of offshore wind turbine monopiles. Procedia Engineering 199, 3230-3235 (2017).
12. Ju, S-H., Huang, Y-C.: Analyses of offshore wind turbine structures with soil-structure interaction under earthquakes. Ocean Engineering (187), 106-190 (2019).
13. Byrne, B.W., Houlsby, G.T., Burd, H.J., Gavin, K.G., Igoe, D.J., Jardine, R.J., et al.: PISA design model for monopiles for offshore wind turbines: application to a stiff glacial clay till. Géotechnique 70(11), 1030-1047 (2020).
14. Kallehave, D., Byrne, B.W., LeBlanc Thilsted C., Mikkelsen, K.K.: Optimization of monopiles for offshore wind turbines. Philosophical Transactions of the Royal Society A: Mathematical, Physical and Engineering Sciences 373(2035), 20140100 (2015).
15. Seidel, M.: Substructures for offshore wind turbines-Current trends and developments. Festschrift Peter Schaumann, 363-368 (2014).
16. Ding, H., Liu, Y., Zhang, P., Le, C.: Model tests on the bearing capacity of wide-shallow composite bucket foundations for offshore wind turbines in clay. Ocean Engineering 103, 114-122 (2015).
17. Liu, B., Zhang, Y., Ma, Z., Andersen, K.H., Jostad, H.P., Liu, D., et al.: Design considerations of suction caisson foundations for offshore wind turbines in Southern China. Applied Ocean Research 104, 1023-1058 (2020).
18. Wang, X., Zeng, X., Li, J., Yang, X., Wang, H.. A review on recent advancements of substructures for offshore wind turbines. Energy Conversion and Management 158, 103-119 (2018).
19. Kim, D.H., Lee, S.G., Lee, I.K.: Seismic fragility analysis of 5 MW offshore wind turbine. Renewable Energy 65, 250-256 (2016).
20. Asareh, M-A., Schonberg, W., Volz, J.: Fragility analysis of a 5-MW NREL wind turbine considering aero-elastic and seismic interaction using finite element method. Finite Elements in Analysis and Design 120, 57-67 (2016).
21. Prowell, I., Elgamal, A., Lu, J.: Modeling the influence of soil structure interaction on the seismic response of a 5 MW wind turbine. In: 5th International Conference on Recent Advances in Geotechnical Earthquake Engineering and Soil Dynamics, No. 5.09a, pp. 1-8 (2020).

22. Yang, Y., Li, C., Bashir, M., Wang, J., Yang, C.: Investigation on the sensitivity of flexible foundation models of an offshore wind turbine under earthquake loadings. Engineering Structures 183, 756-769 (2019).
23. Gao, B., Ye, G., Zhang, Q., Xie, Y., Yan, B.: Numerical simulation of suction bucket foundation response located in liquefiable sand under earthquakes. Ocean Engineering 235, 1093-1094 (2021).
24. Zheng, X.Y., Li, H., Rong, W., Li, W.: Joint earthquake and wave action on the monopile wind turbine foundation: An experimental study. Marine Structures 44, 125-141 (2015).
25. Yang, Y., Bashir, M., Li, C., Michailides, C., Wang, J.: Mitigation of coupled wind-wave-earthquake responses of a 10 MW fixed-bottom offshore wind turbine. Renewable Energy 157, 1171-1184 (2020).
26. Zhang, J., Cheng, W., Cheng, X., Wang, P., Wang, T.: Seismic responses analysis of suction bucket foundation for offshore wind turbine in clays. Ocean Engineering 232, 109-159 (2021).
27. Sapountzakis, E.J., Dikaros, I.C., Kampitsis, A.E., Koroneou, A.D.: Nonlinear response of wind turbines under wind and seismic excitations with soil–structure interaction. Journal of Computational and Nonlinear Dynamics 10(4), 041007 (2015).
28. Houlsby, G., Kelly, R., Huxtable, J., Byrne, B.: Field trials of suction caissons in clay for offshore wind turbine foundations. Géotechnique 55(4), 287-296 (2005).
29. Huang, M., Liu, L., Shi, Z., Li, S.: Modeling of laterally cyclic loaded monopile foundation by anisotropic undrained clay model. Ocean Engineering 228, 108915 (2021).
30. Shi, Z., Huang, M.: Intergranular-strain elastic model for recent stress history effects on clay. Computers and Geotechnics 118, 103316 (2020).
31. Shi, Z., Liu, L., Huang, M., Shen, K., Wang B.: Simulation of cyclic laterally-loaded piles in undrained clays accounting for soil small strain characteristics. Ocean Engineering. (under review).
32. Atkinson, J., Richardson, D., Stallebrass, S.: Effect of recent stress history on the stiffness of overconsolidated soil. Géotechnique 40(4), 531-540 (1990).
33. Finno, R.J., Kim, T.: Effects of stress path rotation angle on small strain responses. Journal of Geotechnical and Geoenvironmental Engineering 138(4), 526-534 (2012).
34. Zergoun, M.: Effective stress response of clay to undrained cyclic loading. Ph.D. Thesis, University of British Columbia, (1991).
35. Zergoun, M., Vaid, Y.: Effective stress response of clay to undrained cyclic loading. Canadian Geotechnical Journal 31(5), 714-727 (1994).
36. Li, S.: Total-loading EMSD method and the behavior of laterally loaded single pile in clay. Ph.D. Thesis, Tongji University, (2019) (in Chinese).
37. Li, S., Yu, J., Huang, M., Leung, C.: Application of T-EMSD based p-y curves in the three-dimensional analysis of laterally loaded pile in undrained clay. Ocean Engineering 206, 107256 (2020).
38. Gazetas G. Seismic response of end-bearing single piles. Soil Dynamics and Earthquake Engineering 3(2), 82-93 (1984).